DOI 10.1515/htmp-2014-0004 — High Temp. Mater. Proc. 2015; 34(1): 1–11

M. A. Flores-Rentería, M. Ortiz-Domínguez, M. Keddam*, O. Damián-Mejía, M. Elias-Espinosa, M. A. Flores-González, S. A. Medina-Moreno, A. Cruz-Avilés and M. Villanueva-Ibañez

A Simple Kinetic Model for the Growth of Fe_2B Layers on AISI 1026 Steel During the Powder-pack Boriding

Abstract: This work focused on the determination of boron diffusion coefficient through the Fe_2B layers on AISI 1026 steel using a mathematical model. The suggested model solves the mass balance equation at the (Fe_2B/substrate) interface. This thermochemical treatment was carried out in the temperature range of 1123–1273 K for a treatment time ranging from 2 to 8 h. The generated boride layers were characterized by different experimental techniques such as light optical microscopy, scanning electron microscopy, XRD analysis and the Daimler-Benz Rockwell-C indentation technique. As a result, the boron activation energy for AISI 1026 steel was estimated as 178.4 kJ/mol. Furthermore, this kinetic model was validated by comparing the experimental Fe_2B layer thickness with the predicted one at a temperature of 1253 K for 5 h of treatment. A contour diagram relating the layer thickness to the boriding parameters was proposed to be used in practical applications.

Keywords: boriding, incubation time, kinetic model, activation energy, adherence

PACS® (2010). 68.47.De, 68.55.A-, 68.55.jd

***Corresponding author: M. Keddam:** Département de Sciences des Matériaux, Faculté de Génie Mécanique et Génie des Procédés, USTHB, B.P. No. 32, 16111 El-Alia, Bab-Ezzouar, Algiers, Algeria. E-mail: keddam@yahoo.fr

M. A. Flores-Rentería, M. A. Flores-González, S. A. Medina-Moreno, A. Cruz-Avilés, M. Villanueva-Ibañez: Universidad Politécnica de Pachuca-UPP, Carretera Pachuca-Cd. Sahagún km. 20, Ex Hacienda de Santa Bárbara, CP 43830, México, Hidalgo

M. Ortiz-Domínguez: Universidad Autónoma del Estado de Hidalgo, Campus Sahagún, Carretera Cd. Sahagún-Otumba s/n, México, Hidalgo

O. Damián-Mejía: Universidad Nacional Autónoma de México-UNAM, Instituto de Investigación en Materiales, Circuito Exterior, s/n Ciudad Universitaria, Coyoacán, CP 04510, México, D. F.

M. Elias-Espinosa: Instituto Tecnológico y de Estudios Superiores de Monterrey-ITESM Campus Santa Fe, Av. Carlos Lazo No. 100, Del. Álvaro Obregón, CP. 01389, México, D. F.

1 Introduction

Boriding is the most widely used thermochemical surface treatment to enhance the mechanical properties such as high surface harness, wear resistance and corrosion resistance of ferrous alloys [1]. The boriding process involves the diffusion of atomic boron into the base steel. This diffusion takes place in the temperature range of 800–1050 °C for a treatment time ranging from 0.5 to 10 h. Due to its small size and high mobility, the atomic boron diffuses into the base steel, and reacts with Fe to form iron borides (i.e. Fe_2B and FeB) in gaseous, solid, or salt media. Several boriding methods are available such as gas boriding, liquid boriding, plasma boriding and plasma paste boriding. Among these boriding methods, the powder-pack boriding possesses some important advantages in terms of easy handling, the flexibility with respect to the composition of the powder, minimal equipment and low cost [2–4]. In the powder-pack boriding, the boriding agent is placed in a heat resistant box and samples are embedded in the mixture of powder. In practice, a single Fe_2B is preferred to the bilayer configuration (FeB + Fe_2B) which gives rise to cracking and scaling due to difference in coefficients of thermal expansion of borides and that of base steel [5–7].

The modeling of the growth kinetics in the boriding process was considered as a tool to optimize the boride layer thickness according to the practical use of the borided material. For this purpose, different models were reported in the literature to simulate the growth kinetics of Fe_2B layers grown on different substrates. Some of them assumed a linear boron concentration profile through the Fe_2B layers with and without the inclusion of boride incubation times for Fe_2B phase [8–20].

The aim of the present work was to characterize the boride layers formed on AISI 1026 steel by powder-pack boriding in the temperature range of 1123–1273 K. The kinetic studies were performed to analyze the growth of Fe_2B layers on AISI 1026 steel. A simple kinetic model, based on the mass balance equation at the (Fe_2B/substrate) interface, was used to estimate the boron diffusion

coefficient in the temperature range of 1123–1273 K. The estimated boron activation energy was then compared with the data available in the literature. The present model was validated by comparing the experimental value of boride layer thickness with the predicted one at a temperature of 1253 K for a treatment time of 5 h.

Finally, a contour diagram relating the Fe_2B layer thickness to the boriding parameters (temperature and time) was proposed for practical use of this kind of borided steel.

2 The diffusion model

The model considers the growth of Fe_2B layer on a saturated substrate with boron atoms as illustrated in Figure 1.

The $f(x)$ function is relative to the boron distribution in the ferritic matrix before the nucleation of Fe_2B phase. $t_0^{Fe_2B}$ is the incubation period required to form the Fe_2B phase when the matrix reaches a saturation state with boron atoms. $C_{up}^{Fe_2B}$ denotes the upper limit of boron content in $Fe_2B = (60\times10^3\ \text{mol/m}^3)$, $C_{low}^{Fe_2B}$ is the lower limit of boron content in $Fe_2B = (59.8\times10^3\ \text{mol/m}^3)$ and the point $x(t=t) = \text{v}$ represents the Fe_2B layer thickness [21, 22].

The term C_{ads}^{B} is the effective adsorbed boron concentration during the boriding process [23]. From Figure 1, $a_1 = C_{up}^{Fe_2B} - C_{low}^{Fe_2B}$ defines the homogeneity range of the Fe_2B layer, $a_2 = C_{low}^{Fe_2B} - C_0$ is the miscibility gap and C_0 is the boron solubility in the matrix considered as null [24].

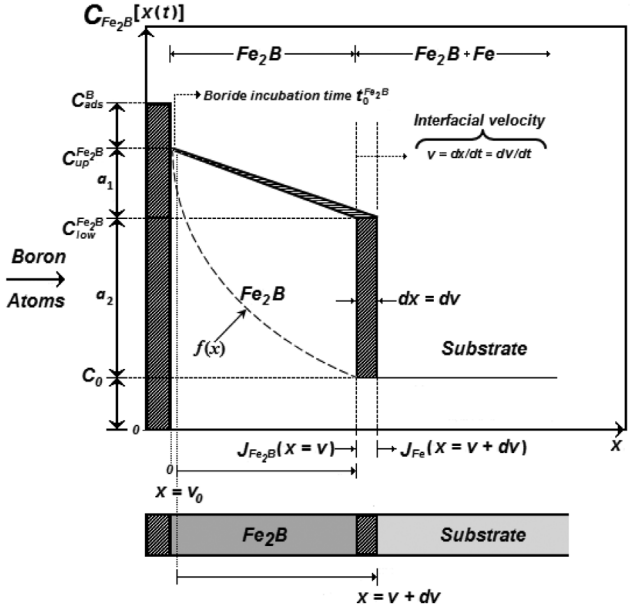

Fig. 1: A schematic boron-concentration profile through the Fe_2B layer.

The following assumptions are taken into account during the establishment of the kinetic model:

- The formation of Fe_2B layer is considered as a one dimensional semi-infinite diffusion problem.
- The growth kinetics is controlled by the boron diffusion in the Fe_2B layer.
- The Fe_2B iron boride nucleates after a specific incubation time.
- The boride layer grows because of the boron diffusion perpendicular to the specimen surface.
- Boron concentrations remain constant in the boride layer during the treatment.
- The influence of the alloying elements on the growth kinetics of the layer is not taken into account.
- The diffusion depth is much smaller than the sample thickness.
- A uniform temperature is assumed throughout the sample.
- Planar morphology is assumed for the phase interface.

The initial and boundary conditions for the diffusion problem are given by:

$$t = 0, x > 0, \text{ with: } C_{Fe_2B}[x(t), t = 0] = C_0 \approx 0. \tag{1}$$

Boundary conditions:

$$\left.\begin{aligned} &C_{Fe_2B}\left[x\left(t = t_0^{Fe_2B}\right) = \text{v}_0, t = t_0^{Fe_2B}\right] = C_{up}^{Fe_2B} \\ &\text{(the upper boron concentration is kept constant),} \\ &\text{for } C_{ads}^{B} > 60\times10^3\ \text{mol m}^{-3}, \end{aligned}\right\} \tag{2}$$

$$\left.\begin{aligned} &C_{Fe_2B}[x(t = t) = \text{v}, t = t] = C_{low}^{Fe_2B} \\ &\text{(the boron concentration at the interface is kept} \\ &\text{constant), } C_{ads}^{B} < 59.8\times10^3\ \text{mol m}^{-3}, \end{aligned}\right\} \tag{3}$$

v_0 is a thin layer with a thickness of ≈5 nm that formed during the nucleation stage [25]. Thus $\text{v}_0 (\approx 0)$ when compared to the thickness of Fe_2B layer (v). The mass balance equation at the (Fe_2B/substrate) interface can be formulated by Eq. (4) as follows:

$$\left(\frac{C_{up}^{Fe_2B} + C_{low}^{Fe_2B} - 2C_0}{2}\right)(A\cdot d\text{v}) = J_{Fe_2B}(x = \text{v}, t = t)(A\cdot dt) - J_{Fe}(x = \text{v} + d\text{v}, t = t)(A\cdot dt), \tag{4}$$

where $A(=1\cdot1)$ is defined as the unit area and C_0 represents the boron concentration in the matrix. The flux J_{Fe_2B} and J_{Fe} are obtained from the Fick's First law as:

$$J_{Fe_2B}\left[x(t=t)=\mathrm{v},\, t=t\right] = -\left\{D_{Fe_2B}\partial C_{Fe_2B}\left[x(t=t)=\mathrm{v},\, t=t\right]/\partial x\right\}_{x=\mathrm{v}} \quad (5)$$

and

$$J_{Fe}\left[x(t=t)=\mathrm{v}+d\mathrm{v},\, t=t\right] = -\left\{D_{Fe}\partial C_{Fe}\left[x(t=t)=\mathrm{v}+d\mathrm{v},\, t=t\right]/\partial x\right\}_{x=\mathrm{v}+d\mathrm{v}} \quad (6)$$

The term J_{Fe} is null since the boron solubility in the matrix is very low (≈ 0 mol/m³) [24].

Thus, Eq. (4) can be written as:

$$\left(\frac{C_{up}^{Fe_2B}+C_{low}^{Fe_2B}-2C_0}{2}\right)\frac{dx(t)}{dt}\bigg|_{x(t)=\mathrm{v}} = -D_{Fe_2B}\frac{\partial C_{Fe_2B}[x(t=t),t=t]}{\partial x}\bigg|_{x(t)=\mathrm{v}}. \quad (7)$$

If a linear boron concentration profile though the Fe_2B layer is assumed, Fick's Second law is reduced to an ordinary second-order differential equation as follows:

$$\frac{d^2C_{Fe_2B}[x(t)]}{dx^2}=0. \quad (8)$$

By solving Eq. (8), and applying the boundary conditions proposed in Eqs (2) and (3), the distribution of boron concentration in Fe_2B is expressed as:

$$C_{Fe_2B}[x(t)]=\frac{C_{low}^{Fe_2B}-C_{up}^{Fe_2B}}{\mathrm{v}}x+C_{up}^{Fe_2B}. \quad (9)$$

By substituting the derivative of Eq. (9) with respect to the distance $x(t)$ into Eq. (7), Eq. (10) is rewritten as:

$$\left(\frac{C_{up}^{Fe_2B}+C_{low}^{Fe_2B}-2C_0}{2}\right)\frac{d\mathrm{v}}{dt}=D_{Fe_2B}\frac{C_{up}^{Fe_2B}-C_{low}^{Fe_2B}}{\mathrm{v}}, \quad (10)$$

for $0 \le x \le \mathrm{v}$.

By integrating the both terms of Eq. (10), Eq. (11) is deduced:

$$\left(\frac{C_{up}^{Fe_2B}+C_{low}^{Fe_2B}-2C_0}{2}\right)\int_{\mathrm{v}=0}^{\mathrm{v}=\mathrm{v}}\mathrm{v}\,d\mathrm{v}=D_{Fe_2B}\left(C_{up}^{Fe_2B}-C_{low}^{Fe_2B}\right)\int_{t=0}^{t=t}dt. \quad (11)$$

After rearranging Eq. (11), the expression of the parabolic growth law can be obtained as:

$$\mathrm{v}^2=4\varepsilon^2D_{Fe_2B}t=4\varepsilon^2D_{Fe_2B}\left[t_{\mathrm{v}}+t_0^{Fe_2B}\right], \quad (12)$$

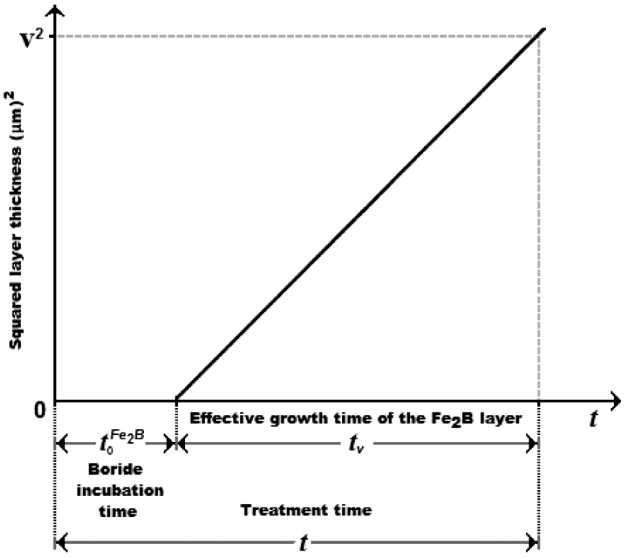

Fig. 2: Schematic representation of the square of the layer thickness against treatment time.

where $\varepsilon^2=\left(C_{up}^{Fe_2B}-C_{low}^{Fe_2B}/C_{up}^{Fe_2B}+C_{low}^{Fe_2B}-2C_0\right)$ is known as the square of normalized growth parameter for the (Fe_2B/substrate) interface, it has no physical dimension. It is assumed that expressions $C_{up}^{Fe_2B}$, $C_{low}^{Fe_2B}$, and C_0, do not depend significantly on temperature (in the temperature range applied) [22]. A schematic depiction of the square of the layer thickness against linear time (see Eq. (12)) is illustrated in Figure 2.

3 Experimental procedure

AISI 1026 steel was used as the substrate material for boriding. It has a nominal chemical composition of 0.22–0.28% C, 0.60–0.90% Mn, 0.07–0.6% Si, 0.050% S, and 0.040% P. The samples were sectioned into cubic samples with dimensions of: 10 mm × 10 mm × 10 mm. Before boriding treatment, samples were ground up to 1200 mesh emery paper and polished. Afterwards, the samples were ultrasonically cleaned in an alcohol solution, acetone and deionized water for 5 min respectively by an ultrasonic cleaner to clean the surfaces. The boriding treatment was carried in the powder mixture consisting of B_4C as a boron source, SiC as an inert filler and KBF_4 as an activator. The boriding process was performed in a conventional furnace under a pure argon atmosphere between 1123 and 1273 K for a treatment time ranging from 2 to 8 h. The samples to be borided were embedded in a closed cylindrical case (AISI 304L) containing a Durborid fresh powder mixture. After the completion of the boriding treatment, the container was removed from the furnace and slowly cooled to

room temperature. The microstructures of polished and etched cross-sections of the boride samples were observed in a clear field by optical microscopy using GX51 Olympus instrument.

The iron boride formed on the surface of borided samples was identified by means of X-ray diffraction (Equinox 2000) using CoK_α radiation at $\lambda = 0.179$ nm. The boride layer thicknesses were automatically measured with the aid of MSQ PLUS software. Fifty measurements were collected in different sections of the borided samples to estimate the boride layer thickness. The distribution of the alloying elements within the boride layer for AISI 1026 steel was confirmed via an Electron Dispersive Spectroscopy (EDS) equipment (JEOL JSM 6300 LV) from the surface to the interior.

The Daimler–Benz Rockwell-C cohesion test [26] was used to assess the adhesion of the boride layers. The well-known Rockwell-C indentation test is prescribed by the VDI 3198 norm, as a destructive quality test for coated compounds. A load of 1471 N was applied to cause coating damage adjacent to the boundary of the indentation. Three indentations were conducted for each specimen. Scanning electron microscopy (JEOL JSM 6300 LV) was employed to evaluate the test.

4 Results and discussions

4.1 Microstructural observations of the boride layers

For investigating the microstructure of borided samples, the borided samples were cut perpendicular to the borides surface using a LECO VC-50 cutting precision machine and embedded in Bakelite. Embedded samples were prepared for metallographic examinations by grinding and polishing (final stage 1 μm diamond paste) followed by etching with 2 vol. % Nital.

In Figure 3 is depicted the optical micrographs of cross-sections of AISI 1026 steel borided at a temperature of 1223 K during 2, 4, 6 and 8 h. The Fe_2B layer was formed on the outer surface of the borided samples, exhibiting a saw tooth morphology. It showed a columnar growth in the all boriding times. When the process time increased, the columnarity became more pronounced and a thicker boride layer was obtained. For analyzing the growth kinetics of Fe_2B layers, the thickness of the boride layers were measured by means of optical microscopy according to the procedure shown in Figure 4. The obtained images were automatically analyzed using MSQ Plus software. In each sample, fifty measurements were done at different points; the reported values were the average thickness of the layers.

The cross-sectional view of SEM micrograph obtained on the borided AISI 1026 steel at 1223 K for 8 h, is shown in Figure 5(a). The Fe_2B layer was formed at the outer surface having a tooth shaped microstructure. The EDS analysis was done at the surface of borided sample (Figure 5 (b)) indicating the presence of Fe element. In fact, iron atoms combine with boron atoms to form the Fe_2B phase if the lower limit of boron concentration is reached in Fe_2B by a mechanism of nucleation and growth of Fe_2B crystals. In Figure 5(c), an EDS analysis was shown at the (Fe_2B/substrate) interface where we can see the four elements: Fe, C, Si and Mn. Carbon and Silicon are diffused towards the diffusion zone by forming together with boron, solid solutions like silicoborides ($FeSi_{0.4}B_{0.6}$ and Fe_5SiB_2) and boroncementite ($Fe_3B_{0.67}C_{0.33}$) [22, 27].

4.2 Formation mechanism of the borided layer

During the powder-pack boriding, the atomic boron released from the powder mixture can be explained by the occurrence of two chemical reactions given in Eqs. (13) and (14):

$$B_4C + 4KBF_4 + 3SiC + 2O_2 \rightarrow 8B\ (\text{adsorption}) + 4KF + 3SiF_4 + 4CO. \quad (13)$$

$$B_4C + 4KBF_4 + 3SiC + 3O_2 \rightarrow 6B\ (\text{adsorption}) + 4KF + 3SiF_4 + 4CO + B_2O_2. \quad (14)$$

If the adsorbed boron concentration exceeds a certain value, the iron atoms react with active boron atoms to form the Fe_2B phase according to the chemical reaction given by:

$$B(adsorption) + 2Fe \rightarrow Fe_2B \quad (15)$$

The Fe_2B phase appears by a mechanism of nucleation and growth. At the beginning, there is a saturation of the matrix by boron element for a time duration corresponding to $t_0^{Fe_2B}$ (see Figure 1). After exceeding this period of incubation, the Fe_2B crystals start to nucleate on the sites energetically favorable. So, the nucleation of Fe_2B crystals at the gas-solid interface is the net result of a competition between the supply of boron from the gas phase and the removal of boron by diffusion into the substrate. The first crystals of Fe_2B grow as needles on the sample surface,

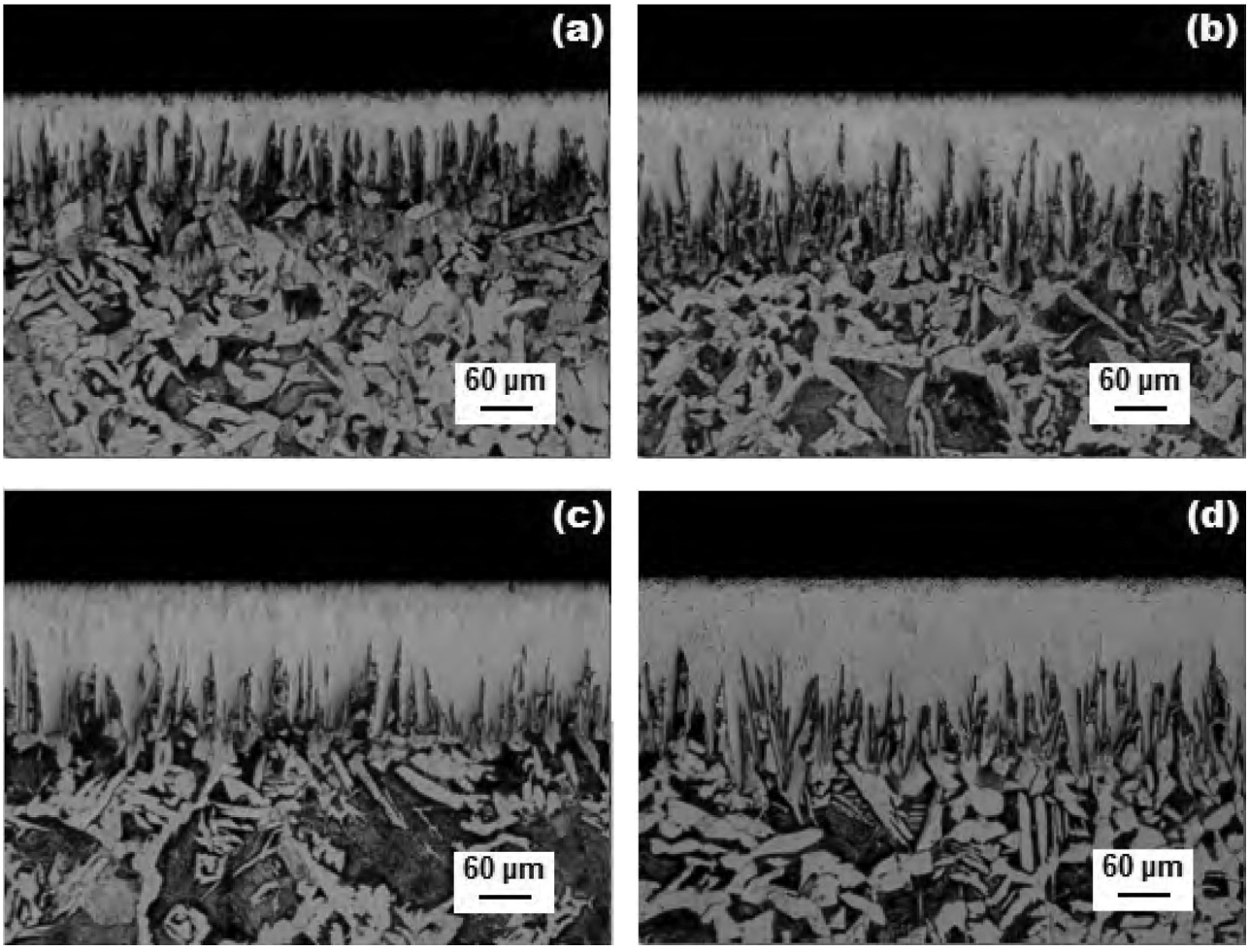

Fig. 3: Optical micrographs of the cross-sections of borided AISI 1026 steel at 1223 K during a variable treatment time: (a) 2 h, (b) 4 h, (c) 6 h and (d) 8 h.

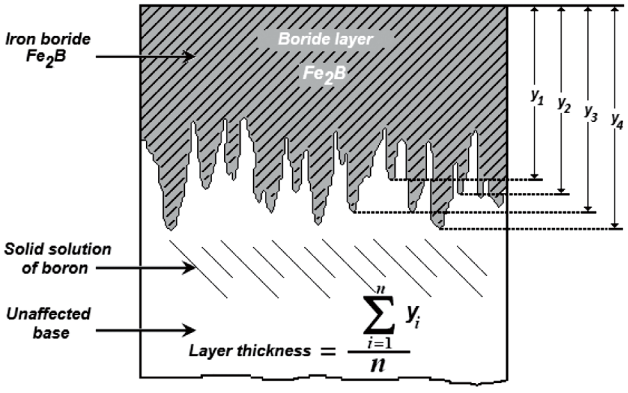

Fig. 4: A Schematic illustration showing the procedure used to estimate the Fe_2B layer thickness on AISI 1026 steel.

starting from the contact zone between the material surface and powder particles.

As a result, the Fe_2B crystals with an acicular shape cover the entire material surface by adopting a textured growth along the [001] direction, following the boron gradient along the boride layer [28–30].

4.3 X-ray diffraction analysis

In Figure 6 is displayed the XRD pattern recorded at the surface of borided AISI 1026 steel after pack-boriding at a temperature of 1273 K for 8 h of treatment. It exhibits the diffracting peaks of Fe_2B phase. Crystals of the Fe_2B type orientate themselves with the z-axis perpendicular to the surface. Consequently, the peaks of the Fe_2B type phases corresponding to crystallographic planes, with deviation from zero of the *l* index, show increased intensities in the X-ray diffraction spectra [31]. It is recognized that the growth of boride layers is a controlled diffusion process with a highly anisotropic nature. In case of the Fe_2B phase, the crystallographic direction [001] is the easiest path for the boron diffusion in the body centered tetragonal crystalline structure of the Fe_2B phase, due to the tendency of

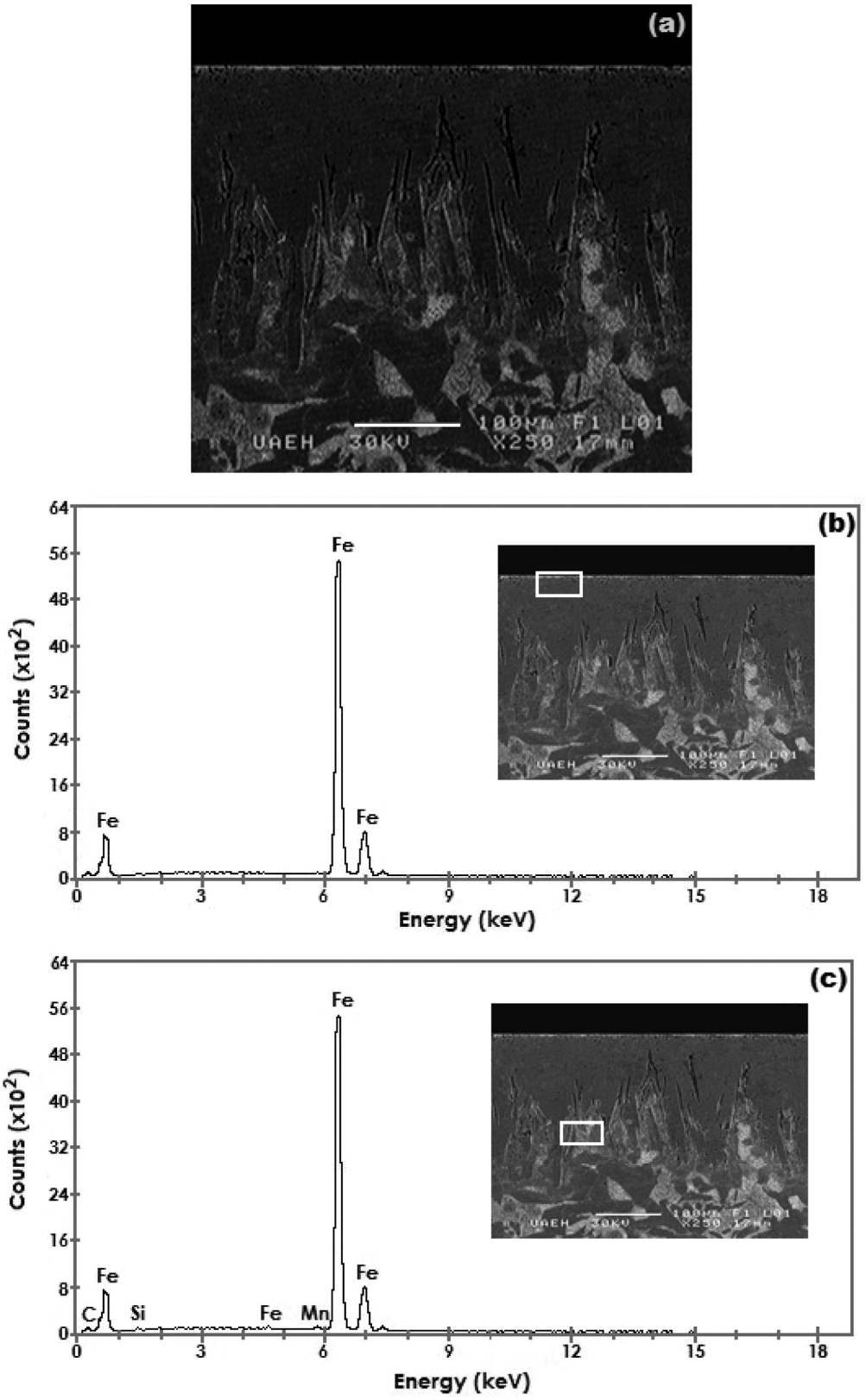

Fig. 5: (a) SEM micrograph of the cross-section of borided AISI 1026 steel at 1223 K for 8 h, (b) EDS spectrum obtained at the surface of borided sample and (c) EDS spectrum obtained at the (boride layer/substrate) interface.

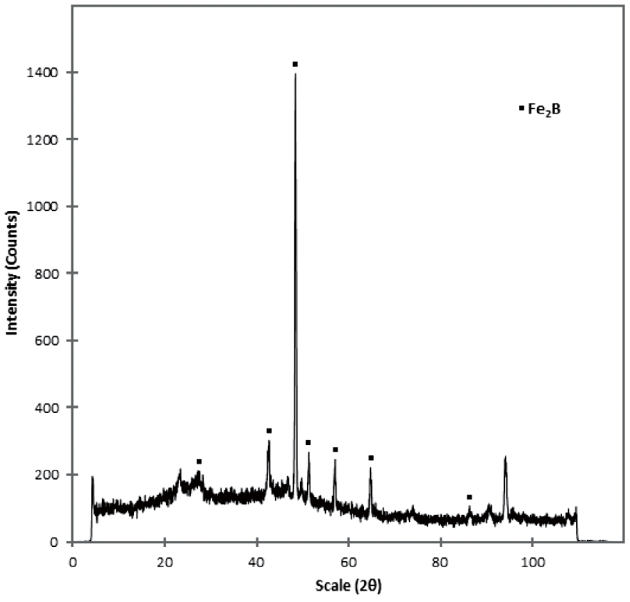

Fig. 6: XRD pattern obtained at the surface of the borided AISI 1026 steel at 1273 K during 8 h of treatment.

boride crystals to grow along a direction of minimum resistance, in the direction of reduction of boron gradient. The occurrence of Fe_2B phase essentially depends on the quantity of active boron in the boron powder. It is reported that using the media with low or intermediate boron potential (as compared to more powerful ones) allow the formation of single Fe_2B layers [32].

4.4 Rockwell-C cohesion

A conical diamond indenter was used to assess the cohesion of the boride layer on AISI 1026 steel using the Daimler-Benz Rockwell-C technique. The well-know cohesion test prescribed by the VDI 3198 norm was used [26] and the principle of this method was presented in Figure 7.

The strength quality of the coated system is established by the following categories: (HF1–HF6) on the basis of a qualitative evaluation. In general, the cohesion strength HF1 to HF4 defined sufficient adhesion, whereas HF5 and HF6 represented insufficient cohesion (HF is the German short form of cohesion strength) [26]. Scanning Electron Microscope (SEM) images of the indentation craters for samples borided at 1273 K for 4 h are given in Figure 8. The indentation craters obtained on the surface of the borided AISI 1026 steel revealed that there were radial cracks at the perimeter of indentation craters. However, a small quantity of spots with flaking of delamination was visible and the cohesion strength quality of this boride layer is related to HF4 category. It is concluded that the presence of Fe_2B phase is responsible of improving the strength quality of the coated system. In this context, it was reported that the (FeB/Fe_2B) bilayer grown on AISI H13 tool steel decreased the adherence of the coated system due to the presence of FeB with tensile residual stresses [33] and flatness of the (boride layer/substrate) interface.

4.5 Estimation of boron activation energy

For estimating the boron diffusion coefficient in the Fe_2B layers at each boriding temperature, it is necessary to plot the variation of the square of Fe_2B layer thickness as a function of the exposure time as depicted in Figure 9. The slopes of the straight lines in this figure represents the

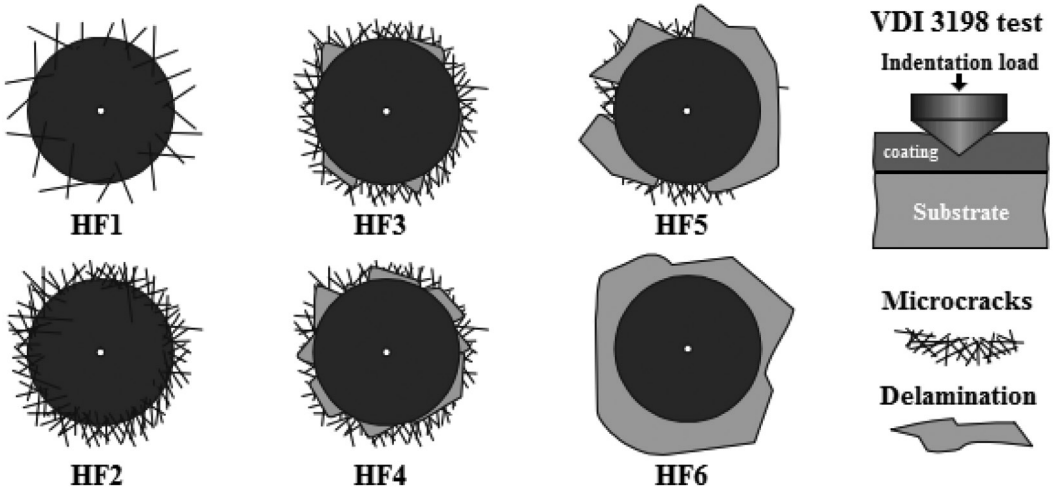

Fig. 7: Principle of the VDI 3198 indentation test [26].

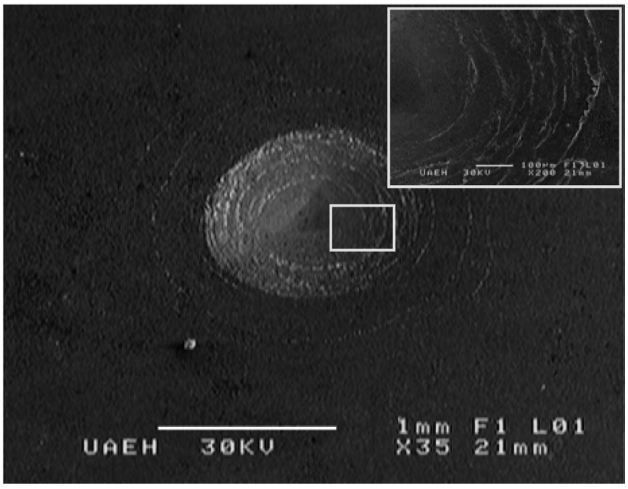

Fig. 8: SEM micrograph showing the indentation of VDI cohesion test on the surface of AISI 1026 steel borided at 1273 K for 4 h.

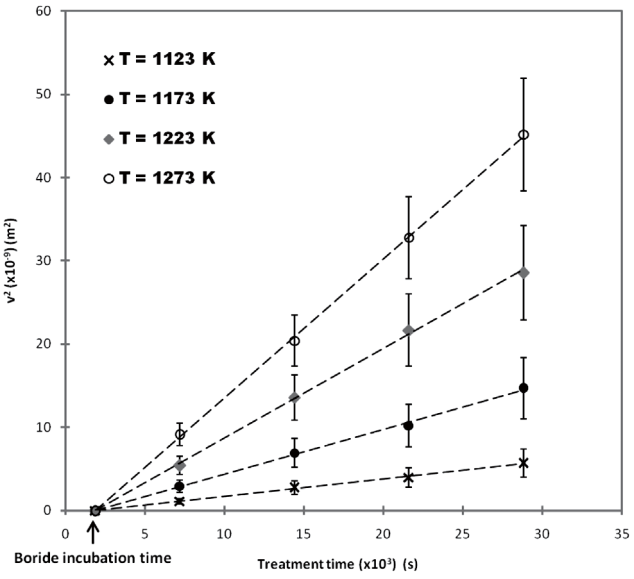

Fig. 9: The square of Fe_2B layer thickness as a function of the boriding time.

growth constants ($=4\varepsilon^2 D_{Fe_2B}$) of the parabolic growth law ($v^2 = 4\varepsilon^2 D_{Fe_2B} t$), where the intercept on the abscissa is taken as the boride incubation time on the graph. The boride incubation time required to form the Fe_2B phase is found independent on temperature. Table 1 gathers the estimated value of boron diffusion coefficient through the Fe_2B layer at each boriding temperature along with the square of ε parameter.

By combining the results (square of normalized growth parameters (ε^2) and growth constants ($4\varepsilon^2 D_{Fe_2B}$)) presented in Table 1, the boron diffusion coefficient in the Fe_2B layers (D_{Fe_2B}) was determined for each boriding temperature. To get the boron activation energy (Q_{Fe_2B}), it is necessary to plot the natural logarithm of (D_{Fe_2B}) as a function of the reciprocal temperature according to the Arrhenius equation (see Figure 10). A linear fitting was adopted to get the temperature dependence of (D_{Fe_2B}) with a correlation factor ($R^2 = 0.9782$).

Table 1: The square of normalized growth parameter and growth constants as a function of boriding temperature.

Temperature (K)	Type of layer	ε^2 (Dimensionless)	$4\varepsilon^2 D_{Fe_2B}$ (μm²/s)
1123	Fe_2B	1.66945×10^{-3}	2.00×10^{-1}
1173	Fe_2B	1.66945×10^{-3}	5.91×10^{-1}
1223	Fe_2B	1.66945×10^{-3}	12.0×10^{-1}
1273	Fe_2B	1.66945×10^{-3}	19.0×10^{-1}

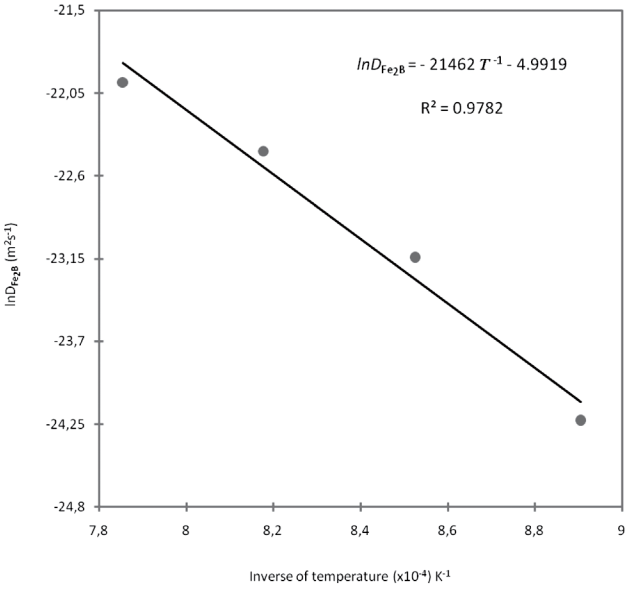

Fig. 10: The temperature dependence of boron diffusion coefficient in the Fe_2B layer.

$$D_{Fe_2B} = 6.8 \times 10^{-3} \exp\left(\frac{-178.4\ kJ/mol}{RT}\right), \qquad (16)$$

where $R = 8.3144621$ J/mol.K and T the absolute temperature in Kevin.

Table 2 compares the value of boron activation energy for AISI 1026 steel with the values found in the literature for some borided steels. It is concluded that the reported values of boron activation energy depended on various factors such as: (the boriding method, the boriding agent and the chemical composition of base steel).

Table 2: A comparison of boron activation energy of AISI 1026 steel with other steels using different boriding methods.

Material	Boriding method	Boron activation energy (kJ/mol)	References
AISI 1020	Powder	110.3	[34]
AISI 1040	Powder	118.8	[34]
AISI 1018	Paste	153	[35]
AISI 1045	Paste	226.7	[36]
Low carbon steel	Electrochemical	175.5	[37]
Low carbon steel	Electrochemical	172.75	[38]
AISI 8620	Plasma paste	99.7–108.8	[39]
AISI 8620	Plasma paste	124.7–138.5	[40]
AISI 1026	Powder	178.4	[present study]

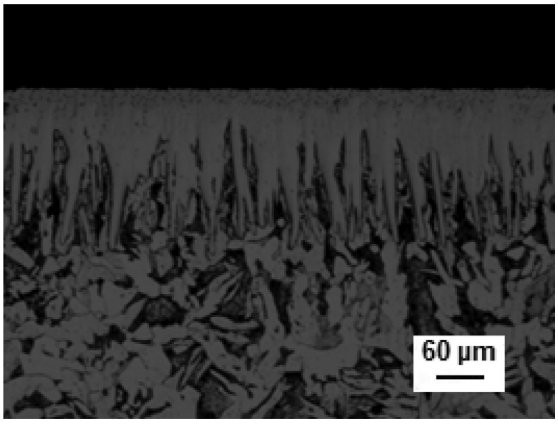

Fig. 11: Optical micrograph of the cross-section of borided AISI 1026 steel at 1253 K during 5 h.

4.6 Experimental validation of the present model

The suggested model was validated by comparing the experimental Fe_2B layer thickness with the predicted one at 1253 K for 5 h using Eq. (17):

$$v = 2\varepsilon D_{Fe_2B}^{1/2} t^{1/2} = \sqrt{\frac{4D_{Fe_2B} t\left(C_{up}^{Fe_2B} - C_{low}^{Fe_2B}\right)}{\left(C_{up}^{Fe_2B} + C_{low}^{Fe_2B} - 2C_0\right)}}. \quad (17)$$

In Figure 11 is shown the optical micrograph of the cross-section of borided AISI 1026 steel at 1253 K during 5 h. Table 3 compares the experimental Fe_2B layer thickness with the predicted value obtained from Eq. (17). A good concordance was observed between the experimental data and the model prediction for a given boriding conditions.

Table 3: Predicted and estimated value of the Fe_2B layer thickness at 1253 K for 5 h of treatment.

Temperature (K)	Type of layer	Boride layer thickness (µm) estimated by Eq. (17)	Experimental boride layer thickness (µm)
1253	Fe_2B	172.09	171.05 ± 11.85

An iso-diagram thickness was also plotted as a function of the temperature and exposure time as shown in Figure 12. This contour plot can be used as a powerful tool to select the optimum value of Fe_2B layer thickness in relation with the potential applications of the borided AISI 1026 steel for industrial applications.

As a rule, thin layers (e.g. 15–20 µm) are used to combat adhesive wear (such as chipless shaping and metal stamping dies and tools), whereas thick layers are recommended to withstand to abrasive wear (extrusion tooling for plastics with abrasive fillers and pressing tools for the ceramic industry). In the case of low carbon steels, the optimum boride layer thicknesses ranges from 50 to 250 µm. Finally, this model can be extended to predict the growth kinetics of bilayer configuration ($FeB + Fe_2B$) grown on any borided steel.

5 Conclusions

In this work, the AISI 1026 steel was pack-borided in the temperature range of 1123–1273 K for a variable exposure time ranging between 2 to 8 h. The concluding points derived from the present work are as follows:

- The Fe_2B layers were formed on AISI 1026 steel. This results was confirmed by XRD analysis
- The growth kinetics of Fe_2B layers followed a parabolic growth law with the presence of incubation boride time independent on the process temperature.
- The interfacial adherence of the boride layer on AISI 1026 steel (obtained at 1273 K during 4 h), by the Daimler-Benz Rockwell-C indentation technique, was found to be related to HF4 category according to VDI 3198 norm.
- A simple kinetic model was proposed for estimating the boron diffusion coefficient in Fe_2B.
- A value of activation energy for AISI 1026 steel was estimated as equal to 178.4 kJ/ mol.
- A useful equation was derived to predict the thickness of the boride layer in the temperature range of 1123–1273 K.

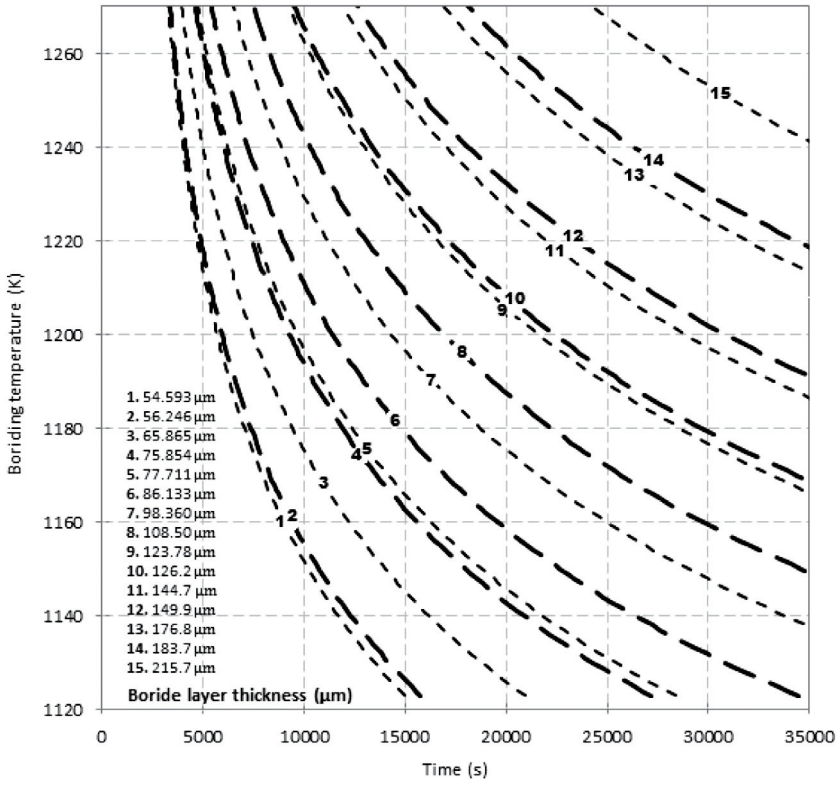

Fig. 12: Contour plot giving the Fe_2B layer thickness as a function of boriding parameters.

- The model was validated by comparing the experimental Fe_2B layer thickness with the predicted one for the sample borided at 1253 K for 5 h. A good agreement was observed for these two set of data.
- A Contour plot relating the boride layer thickness to the boriding parameters (time and temperature) was proposed for practical utilization of this kind of steel. This contour diagram can be used as a tool to select the optimum value of Fe_2B layer thickness.

Nomenclature

v	boride layer thickness (m)
t_v	effective growth time of the Fe_2B layer (s)
t	treatment time (s)
$t_0^{Fe_2B}$	boride incubation time (s)
Q_{Fe_2B}	activation energy of the system (J/mol)
$C_{up}^{Fe_2B}$	upper limit of boron content in Fe_2B ($=60\times10^3$ mol/m^3)
$C_{low}^{Fe_2B}$	lower limit of boron content in Fe_2B ($=59.8\times10^3$ mol/m^3)
C_{ads}^{B}	adsorbed boron concentration in the boride layer (mol/m^3)
a_1	$=C_{up}^{Fe_2B}-C_{low}^{Fe_2B}$; homogeneity range of the Fe_2B layer (mol/m^3)
a_2	$=C_{low}^{Fe_2B}-C_0$; miscibility gap (mol/m^3)
C_0	terminal solubility of the interstitial solute (≈ 0 mol/m^3)
$C_{Fe_2B}[x(t)]$	boron concentration profile in the Fe_2B layer (mol/m^3)
v_0	initial Fe_2B layer (m)
ε	normalized growth parameter for the Fe_2B/substrate interface (no physical dimension)
D_{Fe_2B}	diffusion coefficient of boron in the Fe_2B phase (m^2/s)
$J_i[x(t)]$	(with $i=Fe_2B$ and Fe) fluxes of boron atoms in the Fe_2B/substrate interface boundary (mol/m^2·s)

Acknowledgments: The authors wish to thank the Investigación y Posgrado of the Universidad Politécnica de Pachuca for their valuable collaboration for this study.

Funding: The work described in this paper was supported by a grant of PROMEP and CONACyT México.

Received: January 3, 2014. Accepted: January 18, 2014.

References

[1] A. Graf von Matuschka, *Boronizing*, 1st ed. Munich: Carl Hanser Verlag, 1980.

[2] B. Selcuk, R. Ipek, M.B. Karamis and V. Kuzucu, *J. Mater. Process. Tech.*, 103(2) (2000) 310–317.

[3] I. Campos, G. Ramírez, U. Figueroa, J. Martínez and O. Morales, *Appl. Surf. Sci.,* 253(7) (2007) 3469–3475.

[4] S. Taktak, *Mater. Design.,* 28(6) (2007) 1836–1843.

[5] Z. Lin, Z. Wang and X. Sun, *Wear*, 138(1–2) (1990) 285–294.

[6] C. Bindal and A.H. Üçisik, *Surf. Coat. Tech.,* 122(2–3) (1999) 208–213.

[7] A.H. Ucisik and C. Bindal, *Surf. Coat. Tech.*, 94–95 (1997) 561–565.

[8] D.S. Kukharev, S.P. Fizenko and S.I. Shabunya, *J. Eng. Phys. Therm.*, 69(2) (1996) 187–193.

[9] I. Campos, J. Oseguera, U. Figueroa, J.A. Garcia, O. Bautista and G. Keleminis, *Mater. Sci. Eng. A – Struct.,* 352(1–2) (2003) 261–265.

[10] M. Keddam, *Appl. Surf. Sci.*, 236(1) (2004) 451–455

[11] R. D. Ramdan, T. Takaki and Y. Tomita, *Mater. Trans.,* 49(11) (2008) 2625–2631.

[12] I. Campos-Silva, N. López-Perrusquia, M. Ortiz-Domínguez, U. Figueroa-López, O.A. Gómez-Vargas, A. Meneses-Amador and G. Rodríguez-Castro, *Kovove Mater.*, 47(2) (2009) 75–81.

[13] M. Keddam, M. Ortiz-Domínguez, I. Campos-Silva and J. Martinez-Trinídad, *Appl. Surf. Sci.*, 256(10) (2010) 3128–3132.

[14] M. Ortiz-Domínguez, E. Hernandez-Sanchez, J. Martinez-Trinídad, M. Keddam and I. Campos-Silva, *Kovove Mater.*, 48(5) (2010) 285–290.

[15] M. Keddam and R. Chegroune, *Appl. Surf. Sci.*, 256(16) (2010) 5025–5030.

[16] I. Campos-Silva, M. Ortiz-Domínguez, H. Cimenoglu, R. Escobar-Galindo, M. Keddam, M. Elías-Espinosa and N. López-Perrusquia, *Surf. Eng.*, 27(3) (2011) 189–195.

[17] M. Keddam and R. Chegroune, *Solid State Phenom.*, 170 (2011) 185–189.

[18] Z. Nait Abdellah, M. Keddam and A. Elias, *Defect Diffus. Forum*, 323–235 (2012) 401–406.

[19] Z. Nait Abdellah, M. Keddam, R. Chegroune, B. Bouarour, H. Lillia and A. Elias, *Mat. Tech.,* 100 (2012) 581–588.

[20] Z. Nait Abdellah, M. Keddam and A. Elias, *Int. J. Mater. Res.,* 104 (2013) 260–265.

[21] M. Kulka, N. Makuch, A. Pertek and L. Maldzinski, *J. Solid State Chem.,* 199 (2013) 196–203.

[22] C.M. Brakman, A.W.J. Gommers and E.J. Mittemeijer, *J. Mater. Res*, 4 (1989) 1354–1370.

[23] L.G. Yu, X.J. Chen, K.A. Khor and G. Sundararajan, *Acta Mater.*, 53 (2005) 2361–2368.

[24] Z. Nait Abdellah, R. Chegroune, M. Keddam, B. Bouarour, L. Haddour and A. Elias, *Defect Diffus. Forum*, 322 (2012) 1–9.

[25] V.I. Dybkov, *Reaction Diffusion and Solid State Chemical Kinetics*, Switzerland-UK-USA: Trans Tech Publications, (2010), p. 7.

[26] Verein-Deutscher-Ingenieure, Daimler Benz Adhesion Test, VDI 3198., Dusseldorf: VDI-Verlag, (1992), p. 7.

[27] I.S. Dukarevich, M.V. Mozharov and A.S. Shigarev, *Met. Sci. Heat Treat,* 15(2) (1973) 160–162.

[28] G. Palombarini and M. Carbucicchio, *J. Mater. Sci. Lett.*, 6 (1987) 415–416.

[29] A.J. Ninham and I.M. Hutchings, *J. Vac. Sci. Technol. A*, 4(6) (1986) 2827–2831.

[30] M. Carbucicchio and G. Palombarini, *Hyperfine Interact.*, 83 (1994) 91–110.

[31] C. Badini and D. Mazza, *J. Mater. Sci. Lett.*, 23 (1988) 661–665.

[32] V. Jain and G. Sundararajan, *Surf. Coat. Tech.*, 149(1) (2002) 21–26.

[33] I. Campos-Silva, M. Ortiz-Dominguez, J. Martinez-Trinidad, N. Lopez-Perrusquia, E. Hernandez-Sanchez, G. Ramirez-Sandoval and R. Escobar-Galindo, *Defect Diffus. Forum*, 297–301 (2010) 1284–1289.

[34] O.N. Celik, N. Aydinbeyli and H. Gasan, *Prakt. Metallogr.*, 45(7) (2008) 334–347.

[35] M. Ortiz-Dominguez, I. Campos-Silva, G. Ares de Parga, J. Martinez-Trinidad, M.Y. Jiménez-Reyes, G. Rodriguez-Castro and E. Hernandez-Sanchez, *Kovove Mater.*, 50 (2012) 115–123.

[36] I. Campos, O. Bautista, G. Ramírez, M. Islas, J. de la Parra and L. Zuñiga, *Appl. Surf. Sci.*, 243(1–4) (2005) 429–436.

[37] K. Matiasovsky, M. Chrenkova-Paucirova, P. Fellner and M. Makyta, *Surf. Coat. Tech.*, 35(1–2) (1988) 133–149.

[38] G. Kartal, O.L. Eryilmaz, G. Krumdick, A. Erdemir and S. Timur, *Appl. Surf. Sci.*, 257(15) (2011) 6928–6934.

[39] I. Gunes, S. Ulker, and S. Taktak, *Prot. Met. Phys. Chem.*, 49 (2013) 567–573.

[40] I. Gunes, S. Taktak, C. Bindal, Y. Yalcin, S. Ulker and Y. Kayali, *Sadhana-Acad. P. Eng. S.,* 38(3) (2013) 513–526.